On the Strain Rate Dependence of Hydrogen Embrittlement of High Carbon Steel Assessed by AE

Evgeny D. Merson [1], Dmitri L. Merson [2], Mikhail M. Krishtal [3], Alexei Vinogradov [4]

Abstract: The classic problem of hydrogen-induced cracking (HAC) is revisited aiming at clarification of damage mechanisms leading to failure of hydrogen charged high-carbon steels under load. Plastic deformation and hydrogen-assisted intercrystalline and transcrystalline fracture have been clearly distinguished by AE at different strain rates and discussed.

Keywords: hydrogen-induced cracking, acoustic emission, strain rate.

INTRODUCTION

Hydrogen Assisted Cracking (HAC) is a well-known phenomenon causing substantial degradation of properties in steels and high strength alloys. Particularly, the deteriorative influence of hydrogen is essential for ductility, fracture toughness, fatigue crack growth resistance, etc. At room temperature HAC is particularly pronounced at relatively low strain rates below 10-3 s-1 [1].

The high sensitivity of acoustic emission (AE) technique to HAC has been convincingly demonstrated in a large number of publications, e.g. [2-4]. However no AE studies concerning the strain rate dependence of hydrogen induced damage accumulation have been performed so far to the author's best knowledge despite the fact that HAC is strain rate dependent. Understanding of the interaction between different mechanisms involved into HAC under different strain rates is supposed to shed some light on the mutual role of these mechanisms and their kinetics.

The objective of this work is to determine the effect of hydrogen ingress on the kinetics of HAC in cathodically charged high carbon steel in dependence on the imposed strain rate.

EXPERIMENTAL

High carbon steel 70 in Russian designation (AISI 1070 is a close analogue) was used in the present study since it is known to be prone to premature failure due to HAC. The chemical composition of this steel is shown in Table 1. Samples were mechanically cut to have a rectangular shape of 120×20×1.8 mm dimensions. The samples were thermally treated using a schedule that is commonly used for this type spring steels: quenching from 850±10 ºC in machine oil and tempering at 450±10 ºC for 2 h followed by cooling in air. The hardness after this treatment was of 49±2 HRC.

TABLE 1– *Chemical composition of steel 70.*

C	Si	Mn	Cr	S	P	Cu	Ni	Fe
0.71	0.29	0.59	0.02	0.07	0.10	0.06	0.03	balance

[1] Ph.D. student, Togliatti State University, Belorusskaya 14, 445667, Togliatti, Russia
[2] Professor, Togliatti State University, Belorusskaya 14, 445667, Togliatti, Russia
[3] Professor, Togliatti State University, Belorusskaya 14, 445667, Togliatti, Russia
[4] Assoc. Professor, Osaka City University, Osaka, 558-8585, Japan

For hydrogen charging a part of the specimen was electrolitically plated with a Zn layer of 10 m thick from an alkaline solution containing of 110-120 g/l NaOH and 12-14 g/l ZnO – 12-14. The plating was performed at electric current density of 8 A/dm2 during 20 min. Reference specimens were left unplated for comparison.

Three points bending mechanical testing of the samples with and without coatings was performed at room temperature using a screw driven Instron-type frame. Loading was performed at three different traverse velocities resulting in three different initial strain rates: "slow" - $\dot{\varepsilon}$=3·10-6 s-1, "middle" - $\dot{\varepsilon}$=3·10-4 s-1 and "high" - $\dot{\varepsilon}$=3·10-3 s-1. The ductility was characterized by the maximum value of the deflection at break Δmax.

AE was recorded using a home-made PC-controlled system with a 12 bits ADC at the core. The broadband piezoelectric transducer MSAE-L2 (Microsensors AE, Russia) with a low noise built-in 27dB preamplifier was mounted on the specimen with vacuum oil as a couplant. The signal from the sensor's preamp output was transferred through a main filter-amplifier FA-010 with the 40dB gain and the frequency band 50-1200 kHz. The laboratory noise did not exceed 30 V (peak-to-peak). The burst AE signals with relatively high amplitude above 1 mV (of 30dB threshold) were recorded and counted synchronously with the load signal. The waveforms of 4096 readings were stored for the post-mortem analysis: the energy per realization was calculated from the power spectral density [5]. The true root-mean-square voltage Urms with 100 ms integration time was measured by the FA-010 unit. The Urms signal was fed to a 14 bit ADC for continuous acquisition at 1 kHz sampling rate.

The fracture surface was observed by a scanning electron microscope LEO1455VP.

RESULTS

The ductility of specimens, Δmax, notably reduces after hydrogenation. This is observed at all strain rates, including the highest 3 ɨ10-3 s-1. The effect of embrittlement is much more pronounced at slower strain rates indeed, as is reasonably expected. A similar, but somewhat weaker, negative strain rate dependence of Δmax is also visible for the reference specimens.

TABLE 2— *Ductility Δ_{max} and cumulative AE count N_{Σ}*

Specimen state	Strain rate $\dot{\varepsilon}$, c^{-1}					
	$3\,ɨ10^{-3}$		$3\,ɨ10^{-4}$		$3\,ɨ10^{-6}$	
	Δ_{max}	N_{Σ}	Δ_{max}	N_{Σ}	Δ_{max}	N_{Σ}
Reference	18.3 mm	32	17.3 mm	60	16.9 mm	317
Charged	14.6 mm	84	10.1 mm	385	6.5 mm	5172

The fracture surface of the reference specimens tested at highest strain rate is almost entirely ductile, Fig.1a. The fracture appearance in coated specimens is distinctly different. A typical brittle fracture is observed at the slow strain rate, Fig.1b. Other specimens exhibit fracture patterns of mixed type. The trend seen is that the decrease in $\dot{\varepsilon}$ and/or the increase of H- concentration gives rise to increasing fraction of brittle facets in the fracture relief.

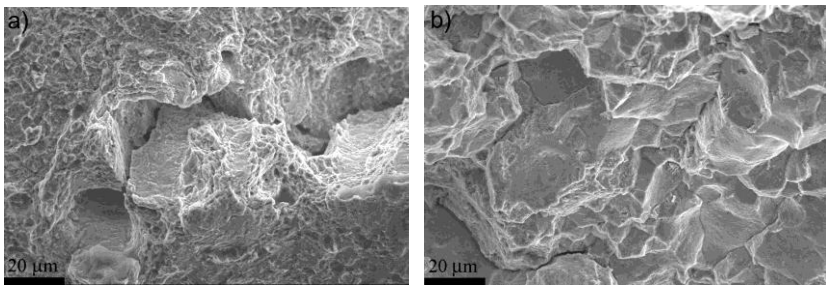

FIG. 1 – SEM images showing fragments of fracture surface of the fractured specimens (a) without coating at $\dot{\varepsilon}$=3 ɨ10-3 s-1 (b) - with coating, at $\dot{\varepsilon}$=3 ɨ10-6 s-1.

As will be shown below, AE in the present steel appears as a mixture of two components: low amplitude continuous and high amplitude burst AE. Uniform plastic deformation caused by dislocation motion in well annealed single- and poly-crystals of pure metals generates a continuous noise-like AE signal [6] . Hence, with increased hardening and reduced ductility the continuous AE component should decrease while the discrete, burst component should increase. Indeed the ductility reduction caused by the strain rate dependent influence of dissolved hydrogen results in the remarkable increase in the number of burst type AE signals during testing (c.f. the total number of discrete events, NΣ , in Table 1).

Apparently, the cumulative AE, NΣ , alone does not represent the whole picture of damage accumulation during straining. Fig. 2 represents the kinetics of AE accumulation in the steel 70 in dependence of the strain rate. The strain rate reduction down to 3·10-6 s-1 gives rise to most rapid AE accumulation which occurs in a step-like manner, e.g. Fig.2a curve 3. The accumulation of AE bursts for hydrogen charged specimens is seen to be gradual and continuous even at low strain rate $\dot{\varepsilon}$=3·10-6 s-1 in contrast with the step-like AE accumulation curves for the reference uncoated specimens. This is straightforwardly explained by the fact that the time interval between jumps in the NΣ curve at high concentration of hydrogen is so small that individual jumps become indistinguishable.

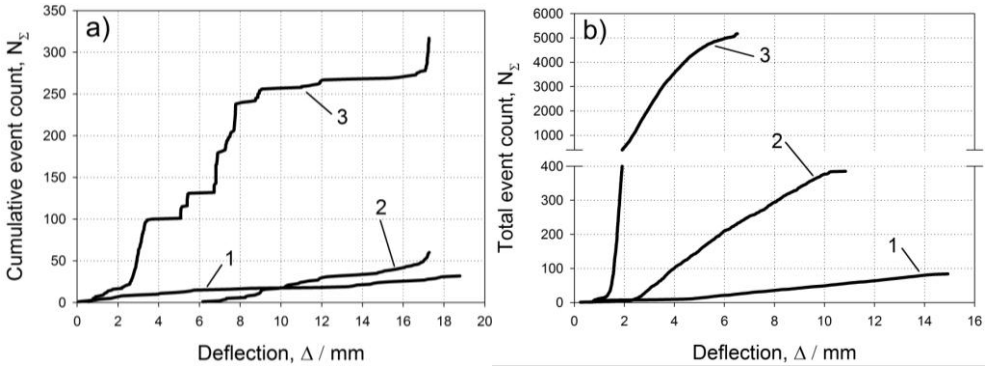

FIG. 2 – Accumulation of discrete AE events and their energy during three point bending testing of the reference (uncoated) specimens (a) and hydrogen charged (coated) specimens (b) at $\dot{\varepsilon}$=3·10-3 s-1 (1), $\dot{\varepsilon}$=3·10-4 s-1 (2) and $\dot{\varepsilon}$=3·10-6 s-1 (3).

The RMS voltage, URMS, shown in Fig.3 reveals a characteristic continuous AE peak in the quasi-elastic part of the loading curve for all specimens (except the reference specimen at lowest $\dot{\varepsilon}$=3·10-6 s-1). However, the AE peak for charged specimens is 5-10 times higher than that for the reference specimens, c.f. also Table 3. Furthermore, the position of the peak is shifted to significantly lower loads after hydrogenation. When $\dot{\varepsilon}$ reduces from 3·10-3 to 3·10-4 s-1 the AE peak height, U*RMS, reduces for all specimens, Fig.3 a-d, which is a common trend in AE [6-7]. However, U*RMS reduction occurs significantly differently for

two types specimens: in the reference specimens U*RMS decreased by a factor of 10 whereas in the charged specimens this reduction was by far smaller, Table 3. The position of the U*RMS peak with respect to the loading curve does not change substantially. However, the load corresponding to the AE onset, P*AE increases when the strain rate decreases. This load in hydrogen charged specimens is consistently smaller than that in reference specimens. The further decrease in $\dot{\varepsilon}$ by two orders of magnitude to 3·10-6 s-1 results in complete vanish of continuous AE for both types samples. However, the hydrogen charged specimens still exhibit a pronounced AE peak which is created by a large amount of intensive bursts, Fig.3f. If compared to a higher strain rate $\dot{\varepsilon}$=3·10-4 s-1, Fig.3d, the height of the peak is lower by a factor of 2 or 4, while the position of the peak corresponds to a smaller stress, c.f. Table 3.

TABLE 3 – *AE parameters in dependence of the hydrogen charging and strain rate*

State of the specimen	Strain rate $\dot{\varepsilon}$, s^{-1}								
	$3 \cdot 10^{-3}$			$3 \cdot 10^{-4}$			$3 \cdot 10^{-6}$		
	AE peak height, U^*_{RMS}, V	Load of AE onset, P_{AE}, N	Load of AE maximum, P^*_{AE}, N	AE peak height, U^*_{RMS}, V	Load of AE onset, P_{AE}, N	Load of AE maximum, P^*_{AE}, N	AE peak height, U^*_{RMS}, V	Load of AE onset, P_{AE}, N	Load of AE maximum, P^*_{AE}, N
Reference	0.35	731	1266	0.04	1166	1284	-	-	-
Charged	2.10	150	590	0.33	700	984	0.08	256	631

DISCUSSION

We have seen that the ductility reduction caused by hydrogenation or/and strain rate reduction is accompanied by increasing of brittle fraction, Fig.1, and amount of discrete type AE recorded during testing. It is therefore plausible to state that these AE transient signals are originated from microscopic fracture processes such as intergranular cracking along the boundaries separating austenitic grains and decohesion of non-metallic inclusions, The role of sulfide inclusions in the AE accompanying fracture of steels has been highlighted in [8]. The EDS analysis in SEM confirmed that decohesion of MnS inclusions is a primary damaging process in the present steel. Apparently, the number of transient events should scale with intensity of HAC. The strain rate dependence of $N\Sigma$ and Δmax for reference samples is less pronounced than that for hydrogen charged ones. However, the fact that this dependence does take place shows that the reversible HAC [9] can be observed in high strength steels even at very low initial concentration of H atoms which present in steel before plating.

It was noticed that the strain rate reduction down to 3·10-6 s-1 gives rise to most rapid AE accumulation which occurs in a step-like manner. However the AE count reflects only the fact that the local structural transformation, e.g. crack opening, has occurred within the sample, but it does not say anything about the scale of the damage. It has been argued both theoretically and experimentally that the AE amplitude (or r.m.s. voltage, or energy) relates to the size of the defect and its velocity [10]. However, the kinetics of AE energy accumulation for discrete AE signals is similar to that of AE counts, Fig2. This is justified in Fig.4 where $E\Sigma$ is plotted versus $N\Sigma$ for discrete AE signals. The proportionality between these two variables is evident: the linear regression fit is obtained with the correlation coefficient r2>0.98. This makes it reasonable to state that the average energy “per event” is nearly constant during the test, i.e. the conclusion is that the scale of AE generating events remains constant upon loading and variations in the r.m.s voltage are attributed to different activity of AE sources in terms of the number of sources activated per unit time. Different

slopes of the fitting lines show that the average energy "per event" is strain rate dependent: the energy increases with strain rate; however, this dependence is weak and non-linear.

Continuous AE is observed at strain rates of $\dot{\varepsilon}$=3·10-3 and 3·10-4 s-1. This continuous AE forms a pronounced peak in the quasi-elastic region as is commonly observed for a wide range of metals due to plastic (or micro-plastic) deformation [6]. Moreover, it has been well established that the r.m.s voltage of AE caused by uniform plastic deformation should be proportional to $\sqrt{\dot{\varepsilon}}$ [7]. This dependence is however not seen in the reference samples the AE energy appears to be proportional to $\dot{\varepsilon}^2$ and not to $\dot{\varepsilon}$ as could be expected for uniform plastic deformation. The conclusion is that the continuous AE, which is observed in the present work, is not associated with uniform plastic deformation. This seems to be quite reasonable for the present high strength steel.

While in the reference specimens the AE peak is poorly defined at the slow strain rate, the hydrogen charged specimens exhibit a clear AE maximum, compare Figs.3e and f. In the coated samples the AE peak consists of a large number of discrete bursts, which are originated from HAC. At higher strain rates the AE peak in hydrogen charged specimens is also significantly higher than in the reference specimens. This is explained by superposition of continuous AE caused by strongly localized plastic deformation at the tips of the cracks and at inlcusions and burst-type AE associated with brittle crack advance. This superposition of two processes accounts, in particular, for the luck in proportionality between the AE energy peak magnitude and the strain rate in hydrogenated specimens. The intensity of microcracking increases with strain rate reduction in the hydrogen charged specimens, i.e. the contribution of this process in to the resultant AE increases while the continuous AE component reasonably decreases with decreasing strain rate.

CONCLUSIONS

The electrochemical Zn-plating results in hydrogen charging and consequent ductility reduction of a steel 70. The embrittlement is more pronounced with strain rate reduction. This picture is typical of the so-called reversible hydrogen embrittlement which is caused by crack initiation and propagation facilitated by diffusion-active hydrogen [9]. HAC can occur even at very small concentration of dissolved hydrogen.

The cumulative AE event count, NΣ, during three-point bending test of steel 70 specimens depends on their apparent ductility and the fraction of brittle component on the fracture surface. The average energy "per event" is nearly constant during the test, i.e. the scale of the elementary fracture events remains constant upon loading so that variations in the r.m.s. voltage are attributed to different activity of AE sources.

Two competitive mechanisms operate during three-point bending deformation of the high carbon steel 70: (i) localized plastic deformation and (ii) brittle intercrystalline and transcrystalline cracking promoted by hydrogen influence. Both these mechanisms generate AE with markedly different features. When the hydrogen-assisted embrittlement effect is relatively low, the continuous AE associated with strongly localized plastic deformation is dominant. To the contrast, when the effect of hydrogen is significant, AE appears as intensive flow of high amplitude pulses. In the case when both plastic deformation and brittle fracture take place in approximately equal proportions, the mixture of two types AE results either in U*RMS increase or in continues AE superimposed with high energy burst signals.

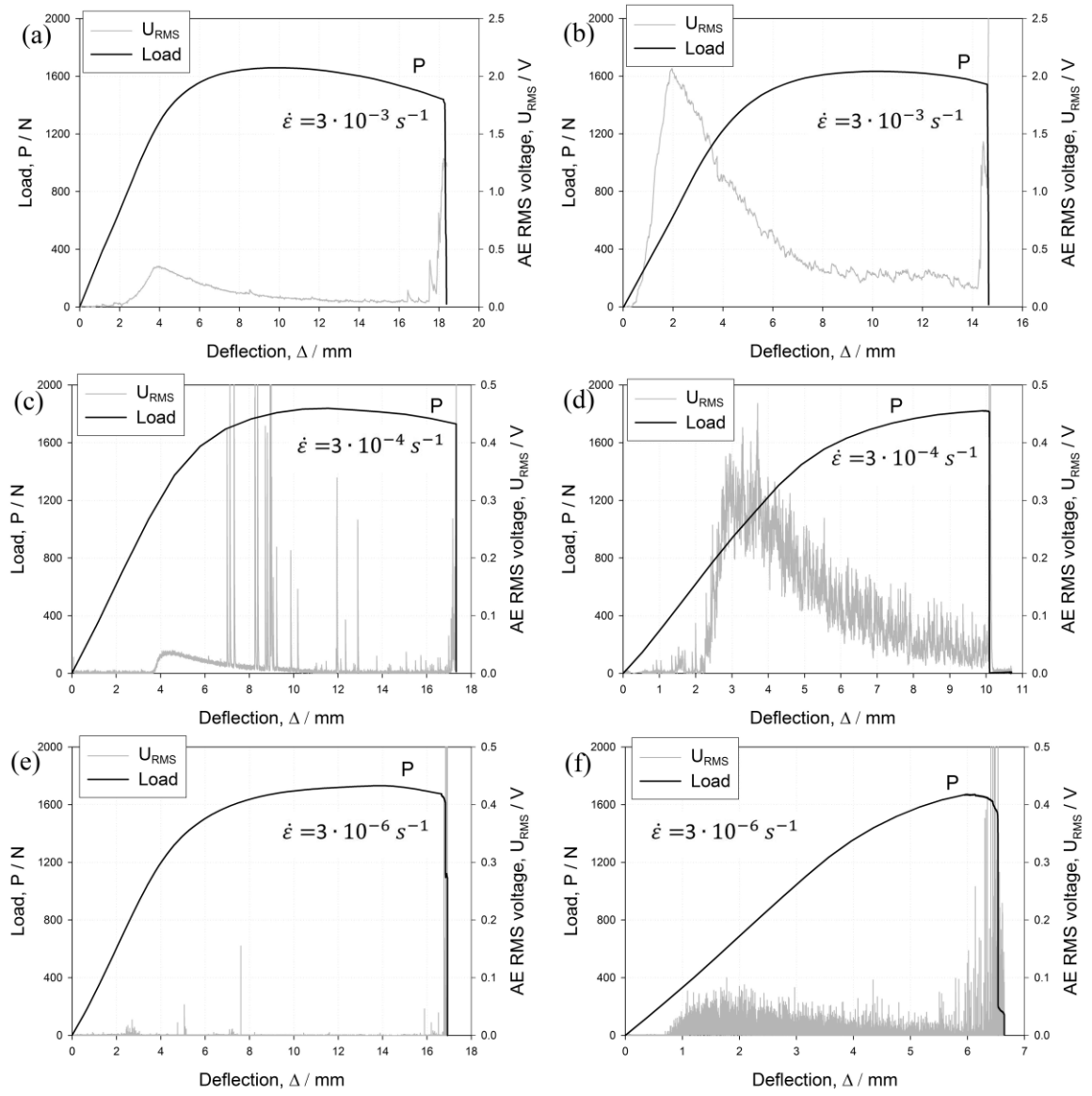

FIG. 3—Typical three-point bending loading curves and AE r.m.s. voltage for the specimens tested at different nominal strain rates: $\dot{\varepsilon}$=3·10-3 s-1 – (a) reference (uncoated) and (b) cathodically charged; $\dot{\varepsilon}$=3·10-4 s-1 (c) reference and (d) cathodically charged; $\dot{\varepsilon}$=3·10-6 s-1 – (e) reference and (f) cathodically charged

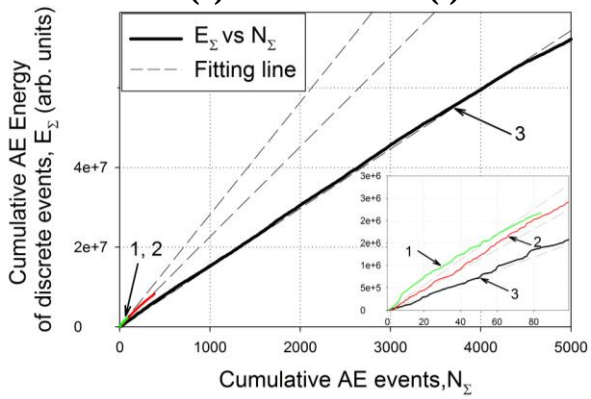

FIG. 4 – Cumulative AE energy of discrete events EΣ vs. cumulative AE events NΣ for hydrogen charged specimens at $\dot{\varepsilon}$=3·10-3 s-1 (1), $\dot{\varepsilon}$=3·10-4 s-1 (2), $\dot{\varepsilon}$=3·10-6 s-1 (3).

ACKNOWLEDGEMENTS

Financial support from the Russian Ministry of Education through the grant-in-aid № 11.G34.31.0031 is greatly appreciated.

REFERENSES

[1] Wu XQ, Kim IS. Mat. Sci. Eng. A 2003;348:309.
[2] Carpenter SH, Smith DR. Met. Trans.A 1990 ;21:1933.
[3] Bhattacharya AK, Parida N, Gope PC. J. Mat.Sci.1992;27:1421.
[4] Merson D, Mesheryakov DE, Vinogradov A. Proc of Int. Symp. on AE, Kyoto, Japan, IAES-19, (2008) 2008. p.115.
[5] Vinogradov A, Nadtochiy M, Hashimoto S, Miura S. Mat.Trans. JIM 1995;36:496.
[6] Heiple CR, Carpenter SH. J. Acoustic Emission. 1987;6:177.
[7] Hatano H. J. Appl. Phys. 1976;47:3873.
[8] Ono K, Yamamoto M. Mat. Sci. Eng. 1981;47:247.
[9] Kolachev BA. Mat. Sci. 979;15:202.
[10] Scruby CB, Wadley HNG, Hill JJ. J. of Phys. D 1983:1069.